Low Complexity Moving Target Parameter Estimation For MIMO Radar using 2D-FFT

Seifallah Jardak*, Sajid Ahmed, *Senior Member, IEEE,* and Mohamed-Slim Alouini, *Fellow, IEEE*
Computer, Electrical, and Mathematical Science and Engineering (CEMSE) Division
King Abdullah University of Science and Technology (KAUST)
Thuwal, Makkah Province, Kingdom of Saudi Arabia
Email: {seifallah.jardak, sajid.ahmed, slim.alouini}@kaust.edu.sa

***Abstract*—In multiple-input multiple-output radar, to estimate the target parameters, such as the reflection coefficient, spatial location, and Doppler shift, derived cost functions are usually optimized over a grid of points. The performance of such algorithms is directly affected by the grid resolution. Increasing the grid resolution enhances the resolution of the estimator but also increases its computational complexity exponentially. In this work, to estimate the parameters of a target, two reduced complexity optimum performance adaptive algorithms, which are based on Capon and amplitude and phase estimation, are presented. The proposed algorithm exploits the low order two-dimensional fast Fourier transform to determine the sub-optimal estimates of spatial location and Doppler shift, which are then used as the initial points for the derived steepest descent algorithm. In contrast to the grid search based algorithms, the proposed algorithm can optimally estimate on- and off-the-grid targets in very low computational complexity. Simulation results show that the mean-squared estimation error of the proposed estimators achieve the Cramér-Rao lower bound.**

***Index Terms*—MIMO-radar, Reflection coefficient, Doppler shift, Spatial location, Cramér-Rao lower bound.**

I. Introduction

In phased array radar, multiple antennas are used to transmit phase-shifted versions of the same waveform to steer the beam in the chosen direction. This increases the reflected power from the target, which as a result increases the signal-to-noise-ratio (SNR) at the receiver and improves the estimation performance of the system. In phased array radar, when a target swerves from its mean position through a small angle, it produces high fluctuations in the SNR at the receiver. This is called scintillation effect and makes target detection challenging. However, the use of independent waveforms provides diversity that can help mitigate scintillation effect [1]. The radar system that emits independent or partially correlated waveforms and uses multiple antennas at the transmitter and the receiver is called a multiple-input multiple-output (MIMO) radar. In MIMO radar, transmitting and receiving antennas can be collocated [2] or widely spaced [3]. In collocated MIMO radar, fully independent waveforms reduce the coherent processing gain, however, they provide extra degrees-of-freedom (DOF), improved spatial resolution, and better parametric identifiability [4]–[6].

This paper is an extended version of the work presented in the International Radar Conference, Lille, France, Oct. 2014. This work was funded by a CRG grant from the KAUST Office of Competitive Research Fund (OCRF).

The main focus of this paper is the collocated MIMO radar. In order to estimate the parameters of stationary targets, such as reflection coefficient and the direction of arrival, using collocated MIMO radar, several adaptive techniques are proposed. For example, in [7] and [8], to jointly estimate the target parameters, a simple one-dimensional search problem is introduced that maximizes a given cost function. For moving targets, in many applications the speed of the target is also required to be estimated, which makes the estimation challenging. Here again, different methods and models have been discussed in the literature. For the widely MIMO radar, a multi-dimensional search problem based on maximum-likelihood (ML) estimator was developed in [9]. Although, it yields optimal performance, its computational complexity is very high, which prevents its use in practice. To reduce the computational complexity of the estimation, sub-optimal algorithms, such as multiple-signal-classification (MUSIC) [10] and estimation-of-signal-parameters-via-rotational-invariant-techniques (ESPRIT) [11], [12] are developed.

Using collocated MIMO radar, the estimation of moving target parameters with ML estimator is a two-dimensional grid search problem. Depending on the grid resolution, the computational complexity of such problems can be very high. To estimate the direction of arrival of moving targets, authors in [13]–[15] have proposed a method, which is based on time division multiplexing.

In the proposed work, using colocated MIMO radar, to estimate the moving target parameters, a low complexity optimal algorithm is proposed. The proposed algorithm is based on both Capon and amplitude-and-phase-estimation (APES) algorithms. The problem of joint estimation of the reflection coefficient, spatial location angle, and Doppler shift is split into two estimation problems. First, a closed-form expression of the reflection coefficient as function of the spatial location and Doppler shift is derived. Next, our manipulation of the cost function allows us to apply the two-dimensional fast-Fourier-transform (2D-FFT) to estimate the Doppler shift and spatial location. This reduces the computational complexity of the two-dimensional grid search problem from $O(N^3)$ to $O(N^2 log_2(N))$. To enhance the resolution of the 2D-FFT estimation, the sub-optimal estimates are used as initial points for the derived steepest descent algorithm, which can also yield off-the-grid estimates. To assess the performance of

the estimators, we compared the mean-square-estimation-error (MSEE) of the parameters with their derived Cramér-Rao lower bound (CRLB). Therefore, in contrast to the conventional algorithms that can only optimally estimate the targets on the grid, our proposed algorithm can optimally estimate the on- and off-the-grid targets.

The organization of the paper is as follows. In the following section the problem is formulated, the estimators of the different parameters are derived in Section III. In Section IV, the Fisher-information-matrix (FIM) and the CRLB of the parameters are derived. Simulation results are presented in Section VI. Finally, conclusion is drawn in Section VII.

Notation: Bold upper case letters, $\mathbf{X}$, and lower case letters, $\mathbf{x}$, respectively denote matrices and vectors. The identity matrix of dimension $n \times n$ is denoted by $\mathbf{I}_n$ and $\mathbf{D}_n^{n+m}$ denotes the diagonal matrix whose elements are $\begin{bmatrix} n & n+1 & \cdots & n+m \end{bmatrix}$. Transpose, conjugate and conjugate transposition of a matrix are respectively denoted by $(\cdot)^T$, $(\cdot)^*$ and $(\cdot)^H$, while the statistical expectation is denoted by $\mathrm{E}\{.\}$. The real, imaginary, and absolute value of a complex variable are respectively represented by $(\cdot)^{\Re}$, $(\cdot)^{\Im}$, and $|x|$.

II. Problem Formulation

Consider a narrowband MIMO radar system with uniform-linear-arrays (ULAs) at the transmitter and the receiver. Let d_T and d_R respectively denote the inter-element spacing between the n_T transmitting and n_R receiving antennas and γ be the ratio d_T/d_R . Let N be the number of moving targets. The ith target is characterized by its reflection coefficient β_{t_i}, its location angle θ_{t_i}, and its normalized Doppler shift $f_{d_{t_i}}$. Each target location can be translated into a normalized spatial frequency defined as $f_{st_i} = \frac{d_R}{\lambda}\sin(\theta_{t_i})$. Moreover, I static interferers, each of reflection coefficient β_i, are located at the normalized spatial frequencies f_{s1} to f_{sI}. If $x_m(l)$ is the baseband signal transmitted from antenna m at time index l, the received signals after matched filter can be expressed in a vector form as

$$\begin{aligned}\mathbf{y}(l) &= \sum_{i=1}^{N} \beta_{t_i} e^{j2\pi f_{d_{t_i}} l} \mathbf{a}_R(f_{st_i}) \mathbf{a}_T^T(fs_{t_i}) \mathbf{x}(l) \\ &+ \sum_{i=1}^{I} \beta_i \mathbf{a}_R(f_{si}) \mathbf{a}_T^T(f_{si}) \mathbf{x}(l) + \mathbf{n}(l),\ l = 0, 1, \ldots, L-1,\end{aligned} \tag{1}$$

where L denotes the total number of symbols transmitted from each antenna and

$$\begin{aligned}\mathbf{a}_T(f_s) &= \begin{bmatrix} 1 & e^{j2\pi\gamma f_s} & \cdots & e^{j2\pi\gamma f_s(n_T-1)} \end{bmatrix}^T, \\ \mathbf{a}_R(f_s) &= \begin{bmatrix} 1 & e^{j2\pi f_s} & \cdots & e^{j2\pi f_s(n_R-1)} \end{bmatrix}^T, \\ \mathbf{x}(l) &= \begin{bmatrix} x_1(l) & x_2(l) & \cdots & x_{n_T}(l) \end{bmatrix}^T, \\ \text{and } \mathbf{n}(l) &= \begin{bmatrix} n_1(l) & n_2(l) & \cdots & n_{n_R}(l) \end{bmatrix}^T,\end{aligned}$$

are respectively the transmit and receive steering vectors corresponding to the normalized spatial frequency f_s, the vector of transmitted symbols at time index l, and the vector of complex white Gaussian noise samples of variance σ_n^2.

III. Proposed Parameter Estimation

Let $\mathbf{R}_{xx}$ be the covariance matrix of the transmitted waveforms, which can be fully independent or partially correlated. To enhance the estimation performance, the received signal is multiplied with a beamformer weight vector, $\mathbf{w}$, after which the received signal can be written as

$$\begin{aligned}\mathbf{w}^H\mathbf{y}(l) &= \sum_{i=1}^{N} \beta_{t_i} e^{j2\pi f_{d_{t_i}} l} \mathbf{w}^H \mathbf{a}_R(f_{st_i}) \mathbf{a}_T^T(f_{st_i}) \mathbf{x}(l) \\ &+ \sum_{i=1}^{I} \beta_i \mathbf{w}^H \mathbf{a}_R(f_{si}) \mathbf{a}_T^T(f_{si}) \mathbf{x}(l) + \mathbf{w}^H \mathbf{n}(l).\end{aligned} \tag{2}$$

In this work, two adaptive beamforming methods are discussed. First, we derive the results for the Capon beamformer [16], [17]. Next, the APES beamformer [18], [19] is discussed.

A. Capon Estimator

The Capon beamformer maximizes the signal-to-interference-plus-noise-ratio (SINR) and helps achieve noise, interference and jamming suppression while keeping the desired signal undistorted. If the covariance matrix of the interference plus noise term is denoted by $\mathbf{R}_{in}$, the SINR is defined as

$$\mathrm{SINR} = \frac{\mathrm{E}\left\{ \left| \sum_{i=1}^{N} \beta_{t_i} e^{j2\pi f_{d_{t_i}} l} \mathbf{w}^H \mathbf{a}_R(f_{st_i}) \mathbf{a}_T^T(f_{st_i}) \mathbf{x}(l) \right|^2 \right\}}{\mathbf{w}^H \mathbf{R}_{in} \mathbf{w}},$$

where

$$\begin{aligned}\mathbf{R}_{in} = \mathrm{E}\Bigg\{ &\left(\sum_{i=1}^{I} \beta_i \mathbf{a}_R(f_{si}) \mathbf{a}_T^T(f_{si}) \mathbf{x}(l) + \mathbf{n}(l) \right) \times \\ &\left(\sum_{i=1}^{I} \beta_i \mathbf{a}_R(f_{si}) \mathbf{a}_T^T(f_{si}) \mathbf{x}(l) + \mathbf{n}(l) \right)^H \Bigg\}.\end{aligned}$$

Using some prior information, one can assume $\mathbf{R}_{in}$ known. However, if it is not the case, the SINR should be expressed using the covariance matrix of the received samples $\mathbf{R}_y$ instead. In both cases, the Capon beamformer is the solution of the following constrained optimization problem [7]

$$\mathbf{w}_{\mathrm{c}} = \begin{cases} \underset{\mathbf{w}}{\operatorname{argmin}}\ \mathbf{w}^H \mathbf{R} \mathbf{w} \\ \text{subject to}\ \ \mathbf{w}^H \mathbf{a}_R(f_s) = 1 \end{cases}, \tag{3}$$

where $\mathbf{R}$ can be $\mathbf{R}_{in}$ or $\mathbf{R}_y$ depending on the discussed case. Solving (3) yields to the following expression of the Capon beamformer

$$\mathbf{w}_c(f_s) = \frac{\mathbf{R}^{-1}\mathbf{a}_R(f_s)}{\mathbf{a}_R^H(f_s)\mathbf{R}^{-1}\mathbf{a}_R(f_s)}. \tag{4}$$

The Capon estimates of f_{dt}, f_{st}, and β_t are defined as the minimizers of the following cost function

$$\begin{aligned}\{\hat{f}_{dt}, \hat{f}_{st}, \hat{\beta}_t\}_c = \underset{f_d, f_s, \beta}{\operatorname{argmin}}\ \mathrm{E}\Big\{ &\left| \mathbf{w}_c^H(f_s)\mathbf{y}(l) \right. \\ &\left. - \beta e^{j2\pi f_d l} \mathbf{a}_T^T(f_s)\mathbf{x}(l) \right|^2 \Big\}.\end{aligned} \tag{5}$$

By differentiating the above expression (5) with respect to β^* and equating it to 0, the minimizing value $\hat{\beta}_c$ can be found as

$$\hat{\beta}_c(f_d, f_s) = \frac{\mathrm{E}\Big\{e^{-j2\pi f_d l}\mathbf{w}_c^H(f_s)\mathbf{y}(l)\mathbf{x}^H(l)\mathbf{a}_T^*(f_s)\Big\}}{P(f_s)}, \quad (6)$$

where

$$P(f_s) = \mathbf{a}_T^T(f_s)\mathbf{R}_{xx}\mathbf{a}_T^*(f_s), \quad (7)$$

is the transmitted power at a normalized spatial frequency f_s. Using (6) in (5), the new cost function used to estimate f_{dt} and f_{st} becomes

$$\begin{aligned} J_1 =& \mathbf{w}_c^H(f_s)\mathbf{R}_y\mathbf{w}_c(f_s) \\ & - \frac{\Big|\mathrm{E}\Big\{e^{-j2\pi f_d l}\mathbf{w}_c^H(f_s)\mathbf{y}(l)\mathbf{x}^H(l)\mathbf{a}_T^*(f_s)\Big\}\Big|^2}{P(f_s)} \\ =& \mathbf{w}_c^H(f_s)\mathbf{R}_y\mathbf{w}_c(f_s) \\ & - \frac{\Big|\mathrm{E}\Big\{e^{-j2\pi f_d l}\mathbf{a}_R^H(f_s)\mathbf{R}^{-1}\mathbf{y}(l)\mathbf{x}^H(l)\mathbf{a}_T^*(f_s)\Big\}\Big|^2}{P(f_s)\left(\mathbf{a}_R^H(f_s)\mathbf{R}^{-1}\mathbf{a}_R(f_s)\right)^2}. \end{aligned} \quad (8)$$

Let us define $\bar{\mathbf{r}}(l) = \mathbf{R}^{-1}\mathbf{y}(l)$. So, the term inside the expectation operator can be written as

$$\begin{aligned} e(l, f_d, f_s) &= e^{-j2\pi f_d l}\mathbf{a}_R^H(f_s)\bar{\mathbf{r}}(l)\mathbf{x}^H(l)\mathbf{a}_T^*(f_s) \\ &= e^{-j2\pi f_d l}\sum_{q=1}^{n_R}\bar{r}_q(l)e^{-j2\pi f_s(q-1)}\sum_{p=1}^{n_T}x_p^*(l)e^{-j2\pi\gamma f_s(p-1)} \\ &= e^{-j2\pi f_d l}\sum_{p=1}^{n_T}\sum_{q=1}^{n_R}\bar{r}_q(l)x_p^*(l)e^{-j2\pi f_s(\gamma(p-1)+q-1)}. \end{aligned}$$

By combining the same frequency terms, we can write

$$\mathrm{E}\{e(l, f_d, f_s)\} = \frac{1}{L}\sum_{l=0}^{L-1}\sum_{n=0}^{\gamma(n_T-1)+n_R-1}\bar{\mathbf{G}}_c(l, n)e^{-j2\pi f_d l}e^{-j2\pi f_s n}, \quad (9)$$

where $\bar{\mathbf{G}}_c(l, n) = \sum_{i=1}^{n_T} x_i^*(l)\bar{r}_{n+1-\gamma(i-1)}(l)$.

Interestingly, the right hand side of (9) is similar to the famous expression of the 2D-FFT. Therefore, by defining the matrix $\mathbf{G}_c = \text{2D-FFT}\left(\bar{\mathbf{G}}_c\right)$, the target's spatial location and Doppler frequency can be jointly estimated as follows

$$\begin{aligned} \{\hat{f}_{dt}, \hat{f}_{st}\}_c = \underset{f_d, f_s}{\operatorname{argmin}} \Bigg[& \mathbf{w}_c^H(f_s)\mathbf{R}_y\mathbf{w}_c(f_s) \\ & - \frac{\left|\frac{1}{L}\mathbf{G}_c(f_d, f_s)\right|^2}{P(f_s)\left(\mathbf{a}_R^H(f_s)\mathbf{R}^{-1}\mathbf{a}_R(f_s)\right)^2}\Bigg]. \end{aligned} \quad (10)$$

As shown in the Appendix, if there are no interferers, minimizing the general Capon cost function (10) becomes equivalent to maximizing its second term only

$$\{\hat{f}_{dt}, \hat{f}_{st}\}_c = \underset{f_d, f_s}{\operatorname{argmax}} \frac{\left|\frac{1}{L}\mathbf{G}_c(f_d, f_s)\right|^2}{P(f_s)\left(\mathbf{a}_R^H(f_s)\mathbf{R}^{-1}\mathbf{a}_R(f_s)\right)^2}. \quad (11)$$

Therefore, in the particular case where fully independent transmit waveforms are used, i.e. $\mathbf{R}_{xx} = I_{n_T}$, and the covariance matrix of the interference plus noise is known, i.e. $\mathbf{R} = \mathbf{R}_{in} = \sigma_n^2 I_{n_R}$, the denominator of the second term becomes constant independent of f_s and the problem in (10) can be further simplified into

$$\{\hat{f}_{dt}, \hat{f}_{st}\}_c = \underset{f_d, f_s}{\operatorname{argmax}} \left|\mathbf{G}_c(f_d, f_s)\right|^2. \quad (12)$$

Finally, a Capon estimator of the target location θ_t can be formulated as

$$\hat{\theta}_{tc} = \sin^{-1}\left(\frac{\lambda}{d_R}\hat{f}_{stc}\right). \quad (13)$$

B. APES Estimator

By following [18], the APES beamformer is formulated as

$$\{\hat{\beta}_t, \mathbf{w}\}_a = \begin{cases} \underset{\beta, \mathbf{w}}{\operatorname{argmin}}\ \mathrm{E}\left\{\left|\mathbf{w}^H(f_s)\mathbf{y}(l) - \beta e^{j2\pi f_d l}\mathbf{a}_T^T(f_s)\mathbf{x}(l)\right|^2\right\}, \\ \text{subject to}\ \ \mathbf{w}^H\mathbf{a}_R(f_s) = 1. \end{cases} \quad (14)$$

Again, by differentiating the cost-function with respect to β^* and equating it to 0, the expression of $\hat{\beta}_a$ will be similar to (6) and the APES beamformer will be the solution of the following problem

$$\begin{aligned} \mathbf{w}_a &= \begin{cases} \underset{\mathbf{w}}{\operatorname{argmin}}\ \mathbf{w}^H \underbrace{\left(\mathbf{R}_y - \frac{\mathbf{v}(f_d, f_s)\mathbf{v}^H(f_d, f_s)}{P(f_s)}\right)}_{\mathbf{V}}\mathbf{w} \\ \text{subject to}\ \ \mathbf{w}^H\mathbf{a}_R(f_s) = 1 \end{cases} \\ &= \frac{\mathbf{V}^{-1}\mathbf{a}_R(f_s)}{\mathbf{a}_R^H(f_s)\mathbf{V}^{-1}\mathbf{a}_R(f_s)}, \end{aligned} \quad (15)$$

where $\mathbf{v}(f_d, f_s) = \mathrm{E}\Big\{e^{-j2\pi f_d l}\mathbf{y}(l)\mathbf{x}^H(l)\mathbf{a}_T^*(f_s)\Big\}$.

The APES estimates of f_{dt} and f_{st} are defined as the minimizers of the below cost function

$$\begin{aligned} \{\hat{f}_{dt}, \hat{f}_{st}\}_a &= \underset{f_d, f_s}{\operatorname{argmin}}\ \mathrm{E}\left\{\left|\mathbf{w}_a^H(f_s)\mathbf{y}(l) - \hat{\beta}_a e^{j2\pi f_d l}\mathbf{a}_T^T(f_s)\mathbf{x}(l)\right|^2\right\} \\ &= \underset{f_d, f_s}{\operatorname{argmin}}\ \mathbf{w}_a^H(f_s)\mathbf{V}\ \mathbf{w}_a(f_s) \\ &= \underset{f_d, f_s}{\operatorname{argmax}}\ \mathbf{a}_R^H(f_s)\mathbf{V}^{-1}\mathbf{a}_R(f_s). \end{aligned} \quad (16)$$

Since $\mathbf{R}_y$ is a full rank matrix, the Sherman-Morrison formula can be used to express the inverse of $\mathbf{V}(f_d, f_s)$ as follows

$$\begin{aligned} \mathbf{V}^{-1}(f_d, f_s) &= \left(\mathbf{R}_y - \frac{\mathbf{v}(f_d, f_s)\mathbf{v}^H(f_d, f_s)}{P(f_s)}\right)^{-1} \\ &= \mathbf{R}_y^{-1} + \frac{\mathbf{R}_y^{-1}\mathbf{v}(f_d, f_s)\mathbf{v}^H(f_d, f_s)\mathbf{R}_y^{-1}}{P(f_s) - \mathbf{v}(f_d, f_s)^H\mathbf{R}_y^{-1}\mathbf{v}(f_d, f_s)}. \end{aligned} \quad (17)$$

Hence, equation (16) becomes equivalent to maximizing

$$\begin{aligned} J_2 = & \mathbf{a}_R^H(f_s)\mathbf{R}_y^{-1}\mathbf{a}_R(f_s) + \\ & \frac{\Big|\mathrm{E}\Big\{e^{-j2\pi f_d l}\mathbf{a}_R^H(f_s)\mathbf{R}_y^{-1}\mathbf{y}(l)\mathbf{x}^H(l)\mathbf{a}_T^*(f_s)\Big\}\Big|^2}{P(f_s) - \mathbf{v}^H(f_d, f_s)\mathbf{R}_y^{-1}\mathbf{v}(f_d, f_s)}. \end{aligned} \quad (18)$$

The expression of the second term's numerator is identical to the one in (8). Hence, the same 2D-FFT approach is again used to evaluate it. Now, a slightly different approach is proposed to compute the quadratic term in the denominator. First, the Cholesky decomposition [20] is used to design an

$$\mathbf{F} = \frac{2n_R}{\sigma_n^2}\sum_{l=0}^{L-1}\begin{pmatrix} p_{0(l,\theta_t)} & 0 & -2\pi l\ \beta_t^{\Im}\ p_{0(l,\theta_t)} & f(1) \\ 0 & p_{0(l,\theta_t)} & 2\pi l\ \beta_t^{\Re}\ p_{0(l,\theta_t)} & f(2) \\ -2\pi l\ \beta_t^{\Im}\ p_{0(l,\theta_t)} & 2\pi l\ \beta_t^{\Re}\ p_{0(l,\theta_t)} & (2\pi l)^2\,|\beta_t|^2\, p_{0(l,\theta_t)} & f(3) \\ f(1) & f(2) & f(3) & f(4) \end{pmatrix}. \tag{28}$$

upper triangular matrix $\mathbf{U}$ such that $\mathbf{U}^H\mathbf{U} = \mathbf{R}_y^{-1}$. Next, by defining the two $n_r \times 1$ column vectors $\tilde{\mathbf{r}}(l) = \mathbf{U}\mathbf{y}(l)$ and $\tilde{\mathbf{v}}(f_d, f_s) = \mathbf{U}\mathbf{v}(f_d, f_s) = \mathrm{E}\Big\{e^{-j2\pi f_d l}\tilde{\mathbf{r}}(l)\mathbf{x}^H(l)\mathbf{a}_T^*(f_s)\Big\}$, we can write

$$\begin{aligned}\tilde{v}_i(f_d, f_s) &= \frac{1}{L}\sum_{l=0}^{L-1}\sum_{n=1}^{n_T}\tilde{r}_i(l)x_n^*(l)e^{-j2\pi f_d l}e^{-j2\pi\gamma f_s(n-1)} \\ &= \frac{1}{L}\sum_{l=0}^{L-1}\sum_{n=0}^{\gamma(n_T-1)}\bar{\mathbf{G}}_a(l,n,i)e^{-j2\pi f_d l}e^{-j2\pi f_s n},\end{aligned} \tag{19}$$

where $\bar{\mathbf{G}}_a(l,n,i) = \tilde{r}_i(l)\bar{x}_n^*(l)$ and

$$\bar{\mathbf{x}}_n = \begin{cases} \mathbf{x}_{\frac{n}{\gamma}+1} & \text{if } n \text{ is a multiple of } \gamma, \\ 0 & \text{otherwise.} \end{cases} \tag{20}$$

By defining the 3D matrix $\mathbf{G}_a = \text{2D-FFT}\left(\bar{\mathbf{G}}_a\right)$, we can finally write

$$\begin{aligned}\mathbf{v}^H(f_d, f_s)\mathbf{R}_y^{-1}\mathbf{v}(f_d, f_s) &= \sum_{i=1}^{n_R}|\tilde{v}_i(f_d, f_s)|^2 \\ &= \sum_{i=1}^{n_R}\left|\frac{1}{L}\mathbf{G}_a(f_d, f_s, i)\right|^2.\end{aligned} \tag{21}$$

Therefore, the cost function in (18) can be reformulated as shown below

$$\{\hat{f}_{dt}, \hat{f}_{st}\}_a = \underset{f_d, f_s}{\text{argmax}}\left[\mathbf{a}_R^H(f_s)\mathbf{R}_y^{-1}\mathbf{a}_R(f_s) + \frac{\left|\frac{1}{L}\mathbf{G}_c(f_d, f_s)\right|^2}{P(f_s) - \sum_{i=1}^{n_R}\left|\frac{1}{L}\mathbf{G}_a(f_d, f_s, i)\right|^2}\right]. \tag{22}$$

In absence of interferers, we showed in the Appendix that the first term of the right hand side expression is minimized at f_{st}. Hence, using a simple proof by contradiction, we can easily conclude that, under the noise only case, maximizing the general APES cost function (22) becomes equivalent to maximizing its second term only

$$\{\hat{f}_{dt}, \hat{f}_{st}\}_a = \underset{f_d, f_s}{\text{argmax}}\ \frac{\left|\frac{1}{L}\mathbf{G}_c(f_d, f_s)\right|^2}{P(f_s) - \sum_{i=1}^{n_R}|\frac{1}{L}\mathbf{G}_a(f_d, f_s, i)|^2}. \tag{23}$$

To asses the performance of the presented estimators, the CRLB of all three parameters will be derived in following section.

IV. Cramér-Rao Lower Bound

In this section, the CRLB is derived in the case where only one moving target is present, i.e. $N = 1$, and can be easily extended for the multiple target case. Let $\boldsymbol{\eta} = \begin{bmatrix} \beta_t^{\Re} & \beta_t^{\Im} & f_{dt} & \theta_t \end{bmatrix}$ be the vector of unknown parameters and $\mathbf{y}$ be the vector where all received samples from time l to $(l+L-1)$ are stacked. Using similar definitions for $\mathbf{u}$ and $\mathbf{n}$, the problem in (1) can be reformulated in a vector form as follows

$$\mathbf{y} = \mathbf{u} + \mathbf{n}, \tag{24}$$

where $\mathbf{y} = \begin{bmatrix}\mathbf{y}^T(l) & \mathbf{y}^T(l+1) & \cdots & \mathbf{y}^T(l+L-1)\end{bmatrix}^T$. Under the assumption that the noise samples are spatially uncorrelated, the FIM for the estimation of $\boldsymbol{\eta}$ can be found using the Slepian-Bangs formula [21]

$$\begin{aligned}\mathbf{F}(\boldsymbol{\eta}) &= \frac{2}{\sigma_n^2}\left(\frac{\partial\mathbf{u}^H}{\partial\boldsymbol{\eta}}\frac{\partial\mathbf{u}}{\partial\boldsymbol{\eta}^T}\right)^{\Re} \\ &= \frac{2}{\sigma_n^2}\sum_{l=0}^{L-1}\left(\frac{\partial\mathbf{u}^H(l)}{\partial\boldsymbol{\eta}}\frac{\partial\mathbf{u}(l)}{\partial\boldsymbol{\eta}^T}\right)^{\Re},\end{aligned} \tag{25}$$

where

$$\frac{\partial\mathbf{u}(l)}{\partial\boldsymbol{\eta}^T} = \begin{bmatrix}\frac{\partial\mathbf{u}(l)}{\partial\beta_t^{\Re}} & \frac{\partial\mathbf{u}(l)}{\partial\beta_t^{\Im}} & \frac{\partial\mathbf{u}(l)}{\partial f_{dt}} & \frac{\partial\mathbf{u}(l)}{\partial\theta_t}\end{bmatrix} \in \mathcal{C}^{n_R\times 4}. \tag{26}$$

Each entry of the vector in (26) can be expressed as follows

$$\begin{aligned}\frac{\partial\mathbf{u}(l)}{\partial\beta_t^{\Re}} &= \mathrm{e}^{j2\pi f_{dt}l}\mathbf{a}_R(\theta_t)\mathbf{a}_T^T(\theta_t)\mathbf{x}(l) = \frac{\mathbf{u}(l)}{\beta_t}, \\ \frac{\partial\mathbf{u}(l)}{\partial\beta_t^{\Im}} &= j\mathrm{e}^{j2\pi f_{dt}l}\mathbf{a}_R(\theta_t)\mathbf{a}_T^T(\theta_t)\mathbf{x}(l) = \frac{\mathbf{u}(l)}{-j\beta_t}, \\ \frac{\partial\mathbf{u}(l)}{\partial f_{dt}} &= j\beta_t 2\pi l\mathrm{e}^{j2\pi f_{dt}l}\mathbf{a}_R(\theta_t)\mathbf{a}_T^T(\theta_t)\mathbf{x}(l) = (j2\pi l)\mathbf{u}(l), \\ \frac{\partial\mathbf{u}(l)}{\partial\theta_t} &= j\beta_t\mathrm{e}^{j2\pi f_{dt}l}2\pi\frac{d_R}{\lambda}\cos(\theta_t)\times \\ &\quad\left(\gamma\mathbf{a}_T^T(\theta_t)\mathbf{D}_0^{n_T-1}\mathbf{x}(l)\mathbf{a}_R(\theta_t) + \mathbf{a}_T^T(\theta_t)\mathbf{x}(l)\mathbf{D}_0^{n_R-1}\mathbf{a}_R(\theta_t)\right).\end{aligned} \tag{27}$$

Thus, using the following notation

$$\begin{aligned}p_0(l,\theta_t) &= \mathbf{a}_T^T(\theta_t)\mathbf{x}(l)\mathbf{x}^H(l)\mathbf{a}_T^*(\theta_t), \\ p_1(l,\theta_t) &= \mathbf{a}_T^T(\theta_t)\mathbf{D}_0^{n_T-1}\mathbf{x}(l)\mathbf{x}^H(l)\mathbf{a}_T^*(\theta_t), \\ p_2(l,\theta_t) &= \mathbf{a}_T^T(\theta_t)\mathbf{D}_0^{n_T-1}\mathbf{x}(l)\mathbf{x}^H(l)\mathbf{D}_0^{n_T-1}\mathbf{a}_T^*(\theta_t),\end{aligned}$$

the FIM corresponding to the estimation of $\boldsymbol{\eta}$ can be represented as in (28). Using the following identity

$$\mathbf{a}_R^H(\theta_t)\left(\mathbf{D}_0^{n_R-1}\right)^k\mathbf{a}_R(\theta_t) = \sum_{n=1}^{n_R-1}n^k, \quad \text{for } k\in\mathbb{N},$$

we can express the term $f(1)$ as shown below

$$\begin{aligned}f(1) &= \frac{1}{n_R}\left(\frac{\mathbf{u}^H(l)}{\beta_t^*}\frac{\partial\mathbf{u}(l)}{\partial\theta_t}\right)^{\Re} \\ &= 2\pi\frac{d_R}{\lambda}cos(\theta_t)\left(j\beta_t\left[\gamma p_{1(l,\theta_t)} + \frac{n_R-1}{2}p_{0(l,\theta_t)}\right]\right)^{\Re} \\ &= -\pi\frac{d_R}{\lambda}cos(\theta_t)\left((n_R-1)\beta_t^{\Im}p_{0(l,\theta_t)} + 2\gamma(\beta_t p_{1(l,\theta_t)})^{\Im}\right).\end{aligned} \tag{29}$$

Similarly, the second term $f(2)$ can be derived as follows

$$\begin{aligned}f(2) &= \frac{1}{n_R}\left(\frac{\mathbf{u}^H(l)}{j\beta_t^*}\frac{\partial\mathbf{u}(l)}{\partial\theta_t}\right)^{\Re} \\ &= \pi\frac{d_R}{\lambda}cos(\theta_t)\left((n_R-1)\beta_t^{\Re}p_{0(l,\theta_t)} + 2\gamma(\beta_t p_{1(l,\theta_t)})^{\Re}\right).\end{aligned} \tag{30}$$

$$\mathbf{F} = \frac{2n_R LP(\theta_t)}{\sigma_n^2} \begin{bmatrix} 1 & 0 & -2\pi S_{10}\beta_t^{\Im} & -\pi\frac{d_R}{\lambda}cos(\theta_t)\times \left((n_R-1)\beta_t^{\Im}+2\gamma(\beta_t S_{01})^{\Im}\right) \\ 0 & 1 & 2\pi S_{10}\beta_t^{\Re} & \pi\frac{d_R}{\lambda}cos(\theta_t)\times \left((n_R-1)\beta_t^{\Re}+2\gamma\Re(\beta_t S_{01})^{\Re}\right) \\ -2\pi S_{10}\beta_t^{\Im} & 2\pi S_{10}\beta_t^{\Re} & (2\pi\left|\beta_t\right|)^2 S_{20} & 2\pi^2\frac{d_R}{\lambda}\left|\beta_t\right|^2 cos(\theta_t)\times \left((n_R-1)S_{10}+2\gamma S_{11}^{\Re}\right) \\ -\pi\frac{d_R}{\lambda}cos(\theta_t)\times \left((n_R-1)\beta_t^{\Im}+2\gamma(\beta_t S_{01})^{\Im}\right) & \pi\frac{d_R}{\lambda}cos(\theta_t)\times \left((n_R-1)\beta_t^{\Re}+2\gamma(\beta_t S_{01})^{\Re}\right) & 2\pi^2\frac{d_R}{\lambda}\left|\beta_t\right|^2 cos(\theta_t)\times \left((n_R-1)S_{10}+2\gamma S_{11}^{\Re}\right) & \left(2\pi\frac{d_R}{\lambda}\left|\beta_t\right|cos(\theta_t)\right)^2\left(\gamma^2 S_{02}+\gamma(n_R-1)S_{01}^{\Re}+\frac{(n_R-1)(2n_R-1)}{6}\right) \end{bmatrix}, \tag{33}$$

$$\mathbf{M} = \left(\mathbf{B}-\mathbf{D}\mathbf{A}^{-1}\mathbf{C}\right)^{-1} = \frac{1}{\pi^2\left(\frac{d_R}{\lambda}\right)^2 cos^2(\theta_t)\alpha} \times \begin{bmatrix} \left(\frac{d_R}{\lambda}\right)^2 cos^2(\theta_t)\left(\gamma^2\left(S_{02}-\left|S_{01}\right|^2\right)+\frac{n_R^2-1}{12}\right) & -\gamma\frac{d_R}{\lambda}cos(\theta_t)\left(S_{11}^{\Re}-S_{01}^{\Re}S_{10}\right) \\ -\gamma\frac{d_R}{\lambda}cos(\theta_t)\left(S_{11}^{\Re}-S_{01}^{\Re}S_{10}\right) & S_{20}-S_{10}^2 \end{bmatrix}, \tag{37}$$

$$\mathbf{Q} = \begin{bmatrix} -\mathbf{A}^{-1}\mathbf{C} \\ \mathbf{I}_{2\times 2} \end{bmatrix} = \begin{bmatrix} 2\pi S_{10}\beta_t^{\Im} & \pi\frac{d_R}{\lambda}cos(\theta_t)\left((n_R-1)\beta_t^{\Im}+2\gamma(\beta_t S_{01})^{\Im}\right) \\ -2\pi S_{10}\beta_t^{\Re} & -\pi\frac{d_R}{\lambda}cos(\theta_t)\left((n_R-1)\beta_t^{\Re}+2\gamma(\beta_t S_{01})^{\Re}\right) \\ 1 & 0 \\ 0 & 1 \end{bmatrix}. \tag{38}$$

Next, the third term $f(3)$ is expressed as follows

$$\begin{aligned} f(3) &= \frac{1}{n_R}\left(\left(-j2\pi l\right)\mathbf{u}^H(l)\ \frac{\partial \mathbf{u}(l)}{\partial\theta_t}\right)^{\Re} \\ &= 4\pi^2\frac{d_R}{\lambda}l\left|\beta_t\right|^2 cos(\theta_t)\left(\gamma p_{1(l,\theta_t)}+\frac{n_R-1}{2}p_{0(l,\theta_t)}\right)^{\Re} \\ &= 2\pi^2\frac{d_R}{\lambda}l\left|\beta_t\right|^2 cos(\theta_t)\left((n_R-1)p_{0(l,\theta_t)}+2\gamma p_{1(l,\theta_t)}^{\Re}\right). \end{aligned} \tag{31}$$

Finally, the last term $f(4)$ is

$$\begin{aligned} f(4) &= \frac{1}{n_R}\left(\frac{\partial \mathbf{u}^H ln)}{\partial\theta_t}\frac{\partial \mathbf{u}(l)}{\partial\theta_t}\right)^{\Re} \\ &= \left|\beta_t\right|^2\left(2\pi\frac{d_R}{\lambda}cos(\theta_t)\right)^2\left(\gamma(n_R-1)p_{1(l,\theta_t)}^{\Re}\right. \\ &\quad \left.+\gamma^2 p_{2(l,\theta_t)}+\frac{(n_R-1)(2n_R-1)}{6}p_{0(l,\theta_t)}\right). \end{aligned} \tag{32}$$

The FIM can then be expressed as in (33) where S_{01}, S_{10}, S_{11}, S_{20}, and S_{02} are defined as

$$S_{nm} = \frac{\sum_{l=0}^{L-1} l^n p_m(l,\theta_t)}{L\ P(\theta_t)},\ \text{for } n,m\in\{0,1,2\}. \tag{34}$$

For notational simplicity, we did not show explicitly the dependence of S_{nm} on θ_t.

Using the matrix inversion lemma

$$\begin{aligned} \begin{bmatrix} \mathbf{A}_{2\times 2} & \mathbf{C}_{2\times 2} \\ \mathbf{D}_{2\times 2} & \mathbf{B}_{2\times 2} \end{bmatrix}^{-1} &= \begin{bmatrix} \mathbf{I}_{2\times 2} \\ \mathbf{0}_{2\times 2} \end{bmatrix}\mathbf{A}^{-1}\begin{bmatrix} \mathbf{I}_{2\times 2} & \mathbf{0}_{2\times 2} \end{bmatrix} \\ &\quad + \begin{bmatrix} -\mathbf{A}^{-1}\mathbf{C} \\ \mathbf{I}_{2\times 2} \end{bmatrix}\left(\mathbf{B}-\mathbf{D}\mathbf{A}^{-1}\mathbf{C}\right)^{-1}\begin{bmatrix} -\mathbf{D}\mathbf{A}^{-1} & \mathbf{I}_{2\times 2} \end{bmatrix}, \end{aligned} \tag{35}$$

the CRLB of the parameters can be found as

$$\text{CRLB}(\boldsymbol{\eta}) = \frac{\sigma_n^2}{2n_R LP(\theta_t)}\left(\begin{bmatrix} \mathbf{I}_{2\times 2} & 0_{2\times 2} \\ 0_{2\times 2} & 0_{2\times 2} \end{bmatrix} + \mathbf{Q}\mathbf{M}\mathbf{Q}^T\right), \tag{36}$$

where $\mathbf{M}$ and $\mathbf{Q}$ are respectively defined in (37) and (38), and

$$\begin{aligned} \alpha &= \left|\beta_t\right|^2\left(S_{20}-S_{10}^2\right)\left(\frac{n_R^2-1}{3}+4\gamma^2\left(S_{02}-\left|S_{01}\right|^2\right)\right) \\ &\quad -4\left|\beta_t\right|^2\gamma^2\left(S_{11}^{\Re}-S_{01}^{\Re}S_{10}\right)^2. \end{aligned} \tag{39}$$

Finally, we can write

$$\begin{aligned} \text{CRLB}\left(\beta_t^{\Re}\right) &= \frac{\sigma_n^2}{2n_R LP(\theta_t)}\left(1+\frac{\Delta_1\ \beta_t^{\Im 2}+\Delta_2\ \beta_t^{\Im}\beta_t^{\Re}+\Delta_3\ \beta_t^{\Re 2}}{\alpha}\right), \\ \text{CRLB}\left(\beta_t^{\Im}\right) &= \frac{\sigma_n^2}{2n_R LP(\theta_t)}\left(1+\frac{\Delta_1\ \beta_t^{\Re 2}-\Delta_2\ \beta_t^{\Im}\beta_t^{\Re}+\Delta_3\ \beta_t^{\Im 2}}{\alpha}\right), \\ \text{CRLB}\left(f_{d_t}\right) &= \frac{\sigma_n^2}{2n_R LP(\theta_t)}\frac{n_R^2-1+12\gamma^2\left(S_{02}-\left|S_{01}\right|^2\right)}{12\pi^2\alpha}, \\ \text{CRLB}\left(\theta_t\right) &= \frac{\sigma_n^2}{2n_R LP(\theta_t)}\frac{S_{20}-S_{10}^2}{\pi^2\left(\frac{d_R}{\lambda}\right)^2\cos^2(\theta_t)\alpha}, \end{aligned} \tag{40}$$

where

$$\begin{aligned} \Delta_1 &= S_{10}^2\left(\frac{n_R^2-1}{3}+4\gamma^2\left(S_{02}-\left|S_{01}\right|^2\right)\right) \\ &\quad +4\gamma S_{10}\left(S_{10}S_{01}^{\Re}-S_{11}^{\Re}\right)\left(n_R-1+2\gamma S_{01}^{\Re}\right) \\ &\quad +\left(S_{20}-S_{10}^2\right)\left(n_R-1+2\gamma S_{01}^{\Re}\right)^2, \\ \Delta_2 &= 8\gamma^2 S_{01}^{\Im}\left(S_{20}S_{01}^{\Re}-S_{10}S_{11}^{\Re}+\frac{n_R-1}{2\gamma}\left(S_{20}-S_{10}^2\right)\right), \\ \Delta_3 &= 4\gamma^2 S_{01}^{\Im\ 2}\left(S_{20}-S_{10}^2\right). \end{aligned} \tag{41}$$

It should be noted that the expressions of the CRLB do not depend on the Doppler shift f_d. To find the optimal estimator $\hat{\boldsymbol{\eta}}$, the solution of (10) and (22) should be determined with very high resolution. Thus, a large number of FFT points should be used to determine the estimates $\hat{f}_d$ and $\hat{f}_s$ as presented in [22]. To reduce the computational cost and avoid using large number of FFT points, an iterative method is presented in the next section.

V. Iterative Method

This method will use low resolution estimates $\hat{f}_{dt}$ and $\hat{f}_{st}$ as initial values to initialize the steepest decent algorithm and optimize the appropriate cost function. Hence, the first order derivatives with respect to f_d and f_s of the following three expressions

$$A(f_d,f_s)=\left|E\Big\{e^{-j2\pi f_d l}\mathbf{a}_R^H(f_s)\mathbf{r}(l)\mathbf{x}^H(l)\mathbf{a}_T^*(f_s)\Big\}\right|^2, \quad (42)$$

$$B(f_d,f_s)=\sum_{i=1}^{n_R}\left|E\Big\{e^{-j2\pi f_d l}\tilde{r}_i(l)\mathbf{x}^H(l)\mathbf{a}_T^*(f_s)\Big\}\right|^2, \quad (43)$$

and

$$C_H(f_s)=\mathbf{a}_R^H(f_s)\ \mathbf{H}\ \mathbf{a}_R(f_s), \quad (44)$$

are required. Here, $\mathbf{H}$ is a generic Hermitian positive semidefinite matrix of size n_R.
Using matrix transformation, we can reformulate (42) as

$$A(f_s,f_d)=\left|\frac{1}{L}\sum_{l=0}^{L-1}e^{-j2\pi f_d l}\mathbf{x}^H(l)\mathbf{M}_r(l)\tilde{\mathbf{a}}^*(f_s)\right|^2, \quad (45)$$

where the i^{th} row of the $n_T\times(n_R+\gamma\,(n_T-1))$ matrix $\mathbf{M}_r(l)$ is defined as

$$(\mathbf{M}_r(l))_i=\Big[\ \underbrace{0\cdots0}_{(i-1)\gamma}\ \mathbf{r}^T(l)\quad 0\cdots0\ \Big],\ i=1,2,\ldots,n_T,$$

and

$$\tilde{\mathbf{a}}(f_s)=\begin{bmatrix}1 & e^{j2\pi f_s} & \cdots & e^{j2\pi f_s(\gamma(n_T-1)+n_R-1)}\end{bmatrix}^T.$$

The derivatives of $A(f_s,f_d)$ with respect to f_d and f_s are respectively computed below

$$\frac{\partial A}{\partial f_d}=-\frac{4\pi}{L^2}\Im\Bigg(\sum_{l=0}^{L-1}e^{-j2\pi f_d l}\mathbf{x}^H(l)\mathbf{M}_r(l)\tilde{\mathbf{a}}^*(f_s)\times \sum_{l=0}^{L-1}l\ e^{j2\pi f_d l}\tilde{\mathbf{a}}^T(f_s)\mathbf{M}_r^H(l)\mathbf{x}(l)\Bigg), \quad (46)$$

$$\frac{\partial A}{\partial f_s}=-\frac{4\pi}{L^2}\Im\Bigg(\sum_{l=0}^{L-1}e^{-j2\pi f_d l}\mathbf{x}^H(l)\mathbf{M}_r(l)\tilde{\mathbf{a}}^*(f_s)\times \sum_{l=0}^{L-1}e^{j2\pi f_d l}\tilde{\mathbf{a}}^T(f_s)\mathbf{D}_0^{\gamma(n_T-1)+n_R-1}\mathbf{M}_r^H(l)\mathbf{x}(l)\Bigg). \quad (47)$$

Next, the derivatives of $B(f_d,f_s)$ can be easily expressed as

$$\frac{\partial B}{\partial f_d}=-\frac{4\pi}{L^2}\sum_{i=1}^{n_R}\Im\Bigg(\Bigg(\sum_{l=0}^{L-1}l\tilde{r}_i^*(l)\mathbf{a}_T^T(f_s)\mathbf{x}(l)e^{j2\pi f_d l}\Bigg)\times \Bigg(\sum_{l=0}^{L-1}\tilde{r}_i(l)\mathbf{x}^H(l)\mathbf{a}_T^*(f_s)e^{-j2\pi f_d l}\Bigg)\Bigg), \quad (48)$$

and

$$\frac{\partial B}{\partial f_s}=-\frac{4\pi\gamma}{L^2}\sum_{i=1}^{n_R}\Im\Bigg(\Bigg(\sum_{l=0}^{L-1}\tilde{r}_i^*(l)\mathbf{a}_T^T(f_s)\mathbf{D}_0^{n_T-1}\mathbf{x}(l)e^{j2\pi f_d l}\Bigg)\times \Bigg(\sum_{l=0}^{L-1}\tilde{r}_i(l)\mathbf{x}^H(l)\mathbf{a}_T^*(f_s)e^{-j2\pi f_d l}\Bigg)\Bigg). \quad (49)$$

Considering the symmetry of $\mathbf{H}$, the third expression $C_H(f_s)$ can be reformulated as follows

$$\begin{aligned}C_H(f_s)&=\sum_{l=1}^{n_R}\sum_{k=1}^{n_R}h_l(k)\mathrm{e}^{j2\pi f_s(k-l)}\\&=\sum_{l=1}^{n_R}h_l(l)+2\Re\left(\sum_{l=1}^{n_R-1}\sum_{k>l}^{n_R}h_l(k)\mathrm{e}^{j2\pi f_s(k-l)}\right)\\&=2\Re\left(\mathbf{h}^T\mathbf{a}_R(f_s)\right),\end{aligned} \quad (50)$$

where

$$\mathbf{h}=\begin{bmatrix}\frac{1}{2}\sum_{l=1}^{n_R}h_l(l) & \sum_{l=1}^{n_R-1}h_l(l+1) & \cdots & h_1(n_R)\end{bmatrix}^T.$$

Consequently, the derivative of C_H with respect to f_s can be expressed as below

$$\frac{\partial C_H(f_s)}{\partial f_s}=-4\pi\Im\left(\mathbf{h}^T\mathbf{D}_0^{n_R-1}\mathbf{a}_R(\theta)\right). \quad (51)$$

Similar to (51), we can easily verify that

$$\frac{\partial P(f_s)}{\partial f_s}=4\pi\gamma\Im\left(\mathbf{r}_{xx}^T\mathbf{D}_0^{n_T-1}\mathbf{a}_T^*(\theta)\right), \quad (52)$$

where

$$\mathbf{r}_{xx}=\begin{bmatrix}\frac{1}{2}\sum_{l=1}^{n_R}\mathbf{R}_{xx}(l,l) & \sum_{l=1}^{n_R-1}\mathbf{R}_{xx}(l,l+1) & \cdots & \mathbf{R}_{xx}(1,n_T)\end{bmatrix}^T.$$

Using the first order derivatives of $A(f_s,f_d)$, $B(f_s,f_d)$, $C_H(f_s)$ and $P(f_s)$, the derivative of the cost functions (10) and (22) defined in Section III can be easily deduced.

VI. Simulation results

This section presents the simulation results and demonstrates the performance of the proposed estimators. In all simulations, 10 transmit and 10 receive antennas are used. The inter-element spacing between antennas at the receiver is set to be half the wavelength, i.e. $d_R=\frac{\lambda}{2}$.

In the first subsection, multiple targets are considered to investigated the effect of the beampattern design on the performance of our algorithms. In the second subsection, we will asses the performance of our estimators by comparing their MSEE with the derived CRLB under different scenarios.

A. Effect of the Beampattern design on the detection performance:

At an SNR= -20 dB, waveforms of L=32 snapshots are transmitted to detect 3 targets with parameters as detailed in Table I. Since there are no interferers, the simplified Capon (11) and APES (23) cost functions are used. After applying a 256 2D-FFT on the simplified cost functions, the results are averaged over 100 realizations. The performance of fully

	θ_t	f_{s_t}	f_{d_t}	β_t
Target 1	$-15°$	-0.129	0.10	$-1+2j$
Target 2	$5°$	0.044	-0.10	$-2-j$
Target 3	$20°$	0.171	0.25	$-2+j$

TABLE I
THE SIMULATION PARAMETERS OF THE MULTIPLE TARGETS

independent waveforms is presented in Fig. 1. In Fig. 2, the beampattern design algorithm proposed in [23] was used to generated 8-PAM signals to maximize the transmitted power between $-30°$ and $30°$.

By comparing the plots (a), (b) and, (c) in Fig. 1, we notice that all three cost functions are maximized around the actual target positions indicated by the red circles. It can also be seen that, when R_{in} is unknown, the peak regions of the Capon cost function is narrower than the ones of the Capon using R_{in} and that the APES maximum regions are even narrower. Moreover, all three plots present a fourth peak which does not correspond to an actual target. However, in Fig. 2, when carefully designed correlated signals are used, the fourth peak is completely suppressed. Hence, the probability of false alarm is reduced. In addition, it should be noted that the peak regions will be narrower at higher SNR values, which requires higher FFT points to detect the maximums.

B. Estimation performance:

In the next simulations, the target of interest is located at $\theta_t = 10°$ and has a reflection coefficient $\beta_t = -1+2j$. Two interferers with reflection coefficients 10 times higher than the SNR are also present at $-10°$ and $30°$. Here, we used $L = 128$ snapshots of fully independent waveforms and the results are averaged over $1,000$ realizations. Since the CRLB of the parameters is independent of target's Doppler shift, for each realization, f_{d_t} is generated from a Gaussian random variable with mean 0.25 and variance 0.001.

Figure 3 presents the performance of the Capon estimator when the interference plus noise covariance matrix R_{in} is known. For this scenario, the peak regions are usually wide, hence a 128 2D-FFT algorithm is used. Figure 3.(a) presents the estimation performance when half-wavelength inter-element spacing is used at the transmitter, i.e. $\gamma = 1$. Because the cost function (10) is also minimized at the location of interferers, we neglected minimums with Doppler shift values around 0. It can be seen that the MSEE of the Doppler shift perfectly matches its CRLB. However, a constant 3 dB gap is present between the MSEE of the spatial location and its CRLB. Besides, in Fig. 3.(b), where a longer virtual array [24]–[27] is constructed by choosing $\gamma = 10$, this gap shrinks considerably. In this case, the CRLB of the Doppler shift remains unchanged while the CRLB of the spatial location expectedly decreases by 20 dB.

Usually, the matrix R_{in} is unknown and the Capon beamformer is computed using R_y. In this scenario, Fig. 4 shows that the MSEE of the spatial location estimator closely follows the CRLB. However, this is not the case for the MSEE of the

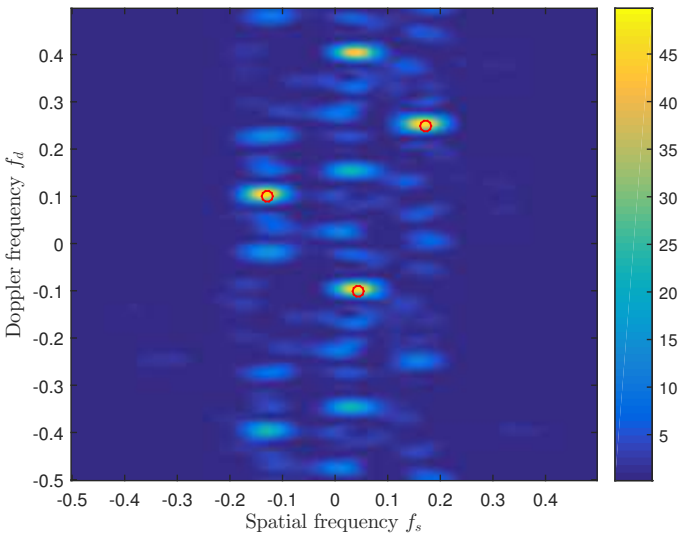

(a) Capon with R_{in} known

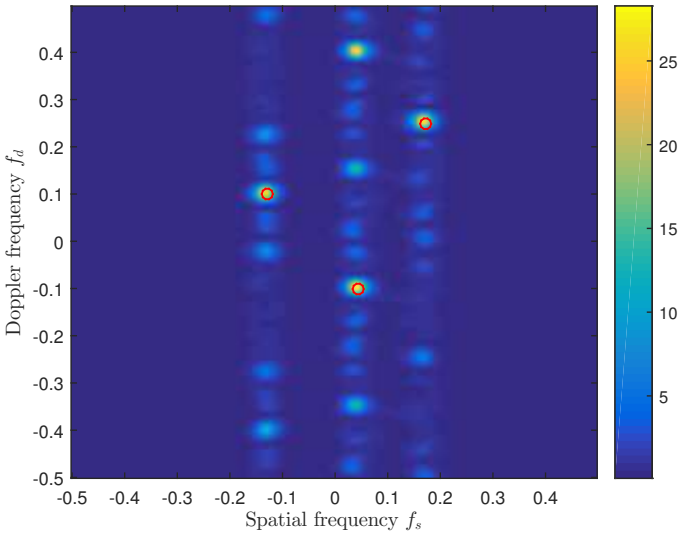

(b) Capon with R_y

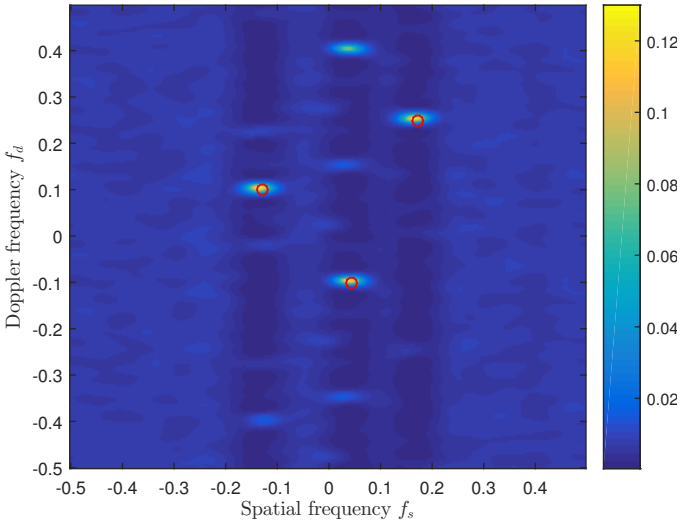

(c) APES

Fig. 1. Amplitude of the different cost functions derived for the (a) Capon with R_{in}, (b) Capon with R_y, and (c) APES algorithms as function of f_d and f_s at SNR$=-20$dB. Three targets are located at the red circles. Here, the transmitted signals are fully independent.

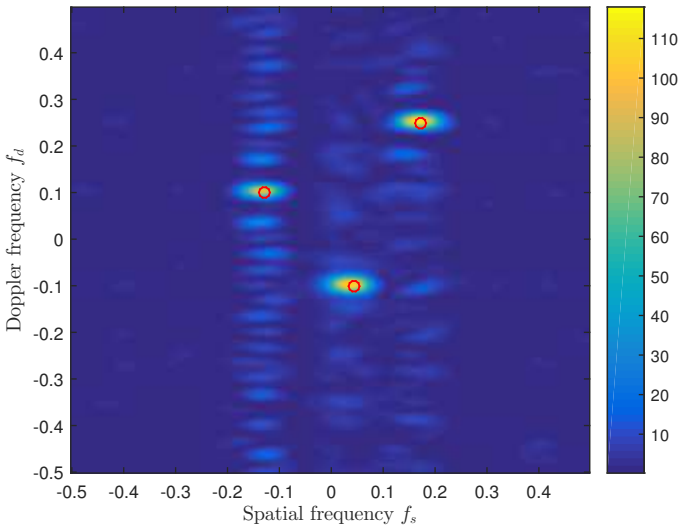

(a) Capon with R_{in} known

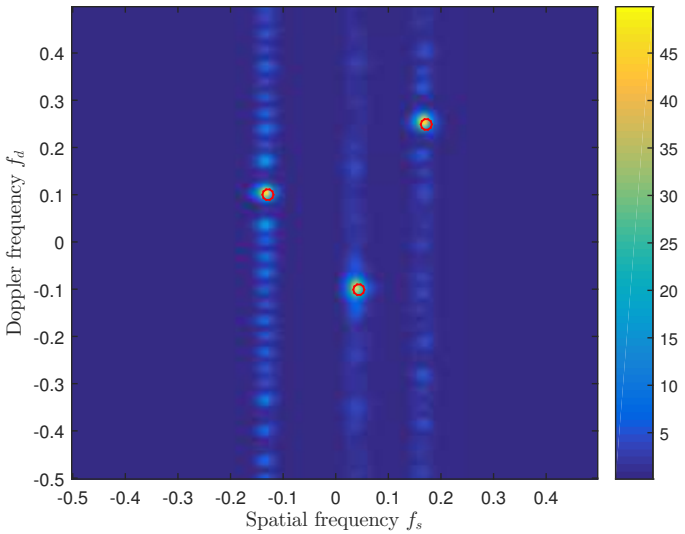

(b) Capon with R_y

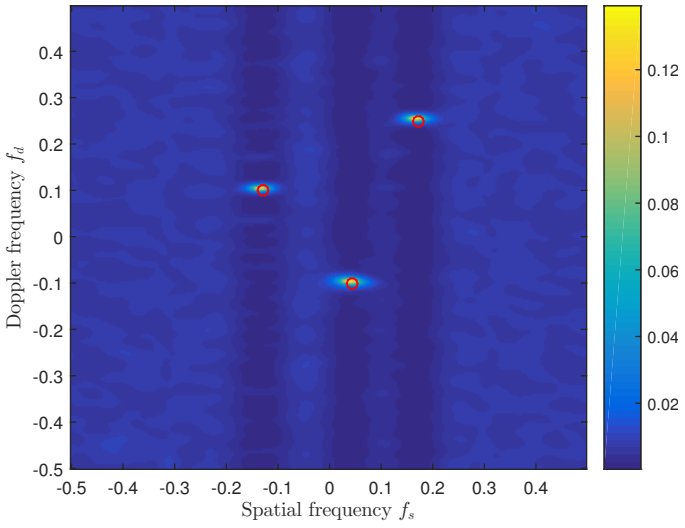

(c) APES

Fig. 2. Amplitude of the different cost functions derived for the (a) Capon with R_{in}, (b) Capon with R_y, and (c) APES algorithms as function of f_d and f_s at SNR$=-20$dB. Three targets are located at the red circles. Here, the transmitted signals are designed to maximize the power beam between -30° and 30°.

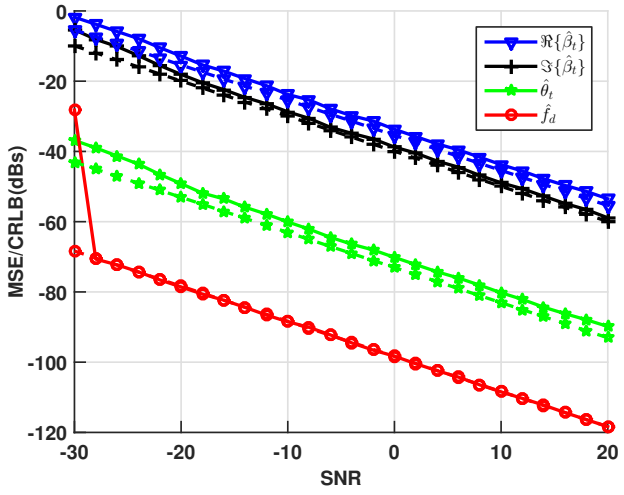

(a) $\gamma = 1$

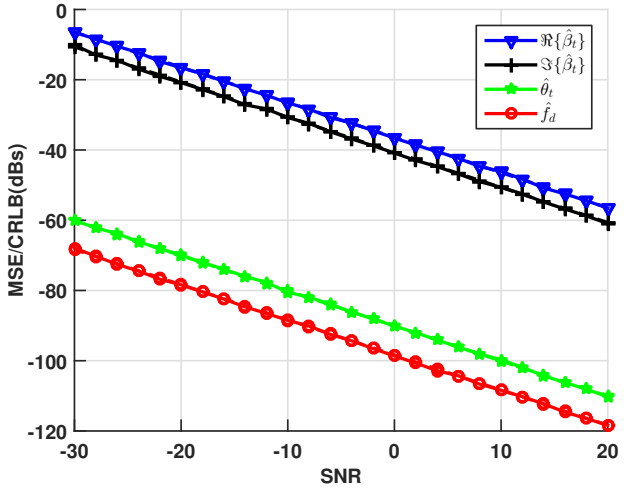

(b) $\gamma = 10$

Fig. 3. Comparison of the CRLB (dashed lines) with the MSEE (solid lines) of the Capon algorithm in the estimation of β_t, f_{dt}, and θ_t using 2D-FFT with 128 points and R_{in} for different values of γ. Here, $\beta_t = -1 + 2j$ and $\theta_t = 10^\circ$.

Doppler shift which is bounded by -75 db while the CRLB is still decreasing.

In [28], where different adaptive algorithms are proposed to estimate the reflection coefficient and the spatial location of non-moving targets, the authors concluded that the APES estimator guarantees better estimation performance compared to the Capon algorithm. This concept remains true when dealing with moving targets. As it can be seen in Fig. 5, the MSEE of both spatial location and Doppler shift frequency meet their respective CRLB graphs. However, this gain in estimation performance comes with a cost in computational complexity. First, as detailed in Section III, although the Capon algorithm requires only one 2D-FFT operation, further 2D-FFT operations are needed to compute the denominator of the APES cost function. Second, to locate the narrower peak regions, higher 2D-FFT orders are required. Hence, to obtain the results in Fig. 5, we used 1024 2D-FFT points for low SNR values and 4096 2D-FFT points for positive SNR values.

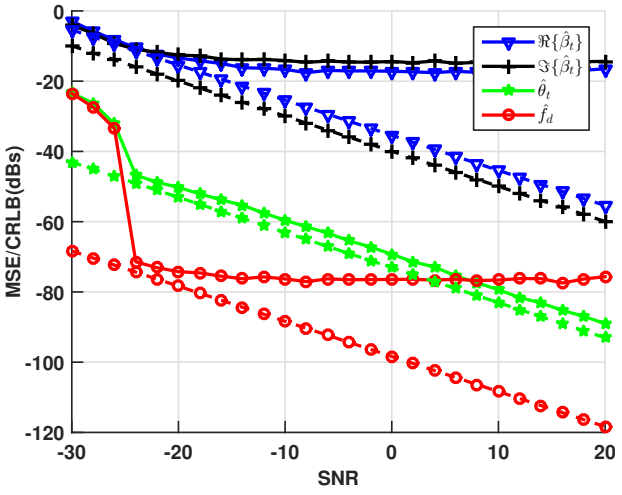

Fig. 4. Comparison of the CRLB (dashed lines) with the MSEE (solid lines) of the Capon algorithm in the estimation of β_t, f_{dt}, and θ_t using 2D-FFT with 1024 points and R_y. Here, $\gamma = 1$, $\beta_t = -1 + 2j$ and $\theta_t = 10°$.

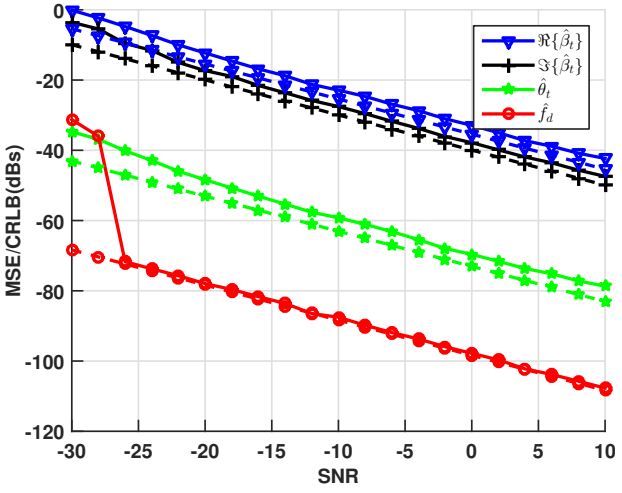

Fig. 5. Comparison of the CRLB (dashed lines) with the MSEE (solid lines) of the APES algorithm in the estimation of β_t, f_{dt}, and θ_t.. Here, $\gamma = 1$, $\beta_t = -1 + 2j$ and $\theta_t = 10°$.

VII. Conclusion

In this work, a low complexity optimal algorithm based on the 2D-FFT is derived for the Capon and APES beamformers to estimate the reflection coefficient, the spatial location and, the Doppler shift of multiple moving targets in presence of static interferes. We also derived the CRLB of these parameters and showed that, when the covariance matrix of the interference plus noise term is known, the MSEE of the Capon estimates achieves the CRLB. However, when only received signals are known, we showed that the APES beamformer provides better estimates than the Capon beamformer at a greater computational cost. To overcome this issue, the combined Capon and APES (CAPES) algorithm can be considered.

Appendix

A two part proof will be derived to demonstrate that, in absence of interferers, minimizing the Capon cost function defined in (10) is equivalent to maximizing its second term (11). In the coming two subsections, we will first prove that

$$\hat{f}_{st} = \underset{f_s}{\operatorname{argmax}}\ \mathbf{w}^H(f_s)\mathbf{R}_y\mathbf{w}(f_s), \tag{A.1}$$

where $\mathbf{w}$ is expressed using $\mathbf{R}_{in}$ or $\mathbf{R}_y$. Later, given (A.1), we will confirm that (10) is equivalent to (11).

A. Capon Beamformer with known $\mathbf{R}_{in}$:

If $\mathbf{R}_{in} = \sigma_n^2\mathbf{I}_{n_R}$ is known, we can write

$$\begin{aligned}\mathbf{w}^H(f_s)\mathbf{R}_y\mathbf{w}(f_s) &= \frac{\mathbf{a}_R^H(f_s)\mathbf{R}_{in}^{-1}\mathbf{R}_y\mathbf{R}_{in}^{-1}\mathbf{a}_R(f_s)}{\left(\mathbf{a}_R^H(f_s)\mathbf{R}_{in}^{-1}\mathbf{a}_R(f_s)\right)^2}\\ &= \frac{\mathbf{a}_R^H(f_s)\mathbf{R}_y\mathbf{a}_R(f_s)}{n_R^2}.\end{aligned} \tag{A.2}$$

Moreover, as the waveforms $\mathbf{x}(n)$ and the noise $\mathbf{v}(n)$ are uncorrelated, the covariance matrix of the received signals $\mathbf{R}_y$ can be derived as below

$$\begin{aligned}\mathbf{R}_y &= \mathrm{E}\left\{\left|\beta_t e^{j2\pi f_{dt}l}\mathbf{a}_R(f_{st})\mathbf{a}_T^T(f_{st})\mathbf{x}(n) + \mathbf{n}(l)\right|^2\right\}\\ &= |\beta_t|^2\,\mathbf{a}_T^T(f_{st})\mathbf{R}_{xx}\mathbf{a}_T^*(f_{st})\ \mathbf{a}_R(f_{st})\mathbf{a}_R(f_{st})^H + \sigma_n^2\mathbf{I}_{n_R}.\end{aligned} \tag{A.3}$$

Therefore, by combining (A.3) and (A.2), we can deduce that

$$\begin{aligned}&\mathbf{w}^H(f_s)\mathbf{R}_y\mathbf{w}(f_s)\\ &= \frac{|\beta_t|^2}{n_R^2}\mathbf{a}_T^T(f_{st})\mathbf{R}_{xx}\mathbf{a}_T^*(f_{st})\left|\mathbf{a}_R^H(f_s)\mathbf{a}_R(f_{st})\right|^2 + \frac{\sigma_n^2}{n_R},\end{aligned} \tag{A.4}$$

which is clearly maximized at $f_s = f_{st}$ □.

B. Capon Beamformer with unknown $\mathbf{R}_{in}$:

If $\mathbf{R}_{in}$ is unknown, we can write

$$\begin{aligned}\mathbf{w}^H(f_s)\mathbf{R}_y\mathbf{w}(f_s) &= \frac{\mathbf{a}_R^H(f_s)\mathbf{R}_y^{-1}\mathbf{R}_y\mathbf{R}_y^{-1}\mathbf{a}_R(f_s)}{\left(\mathbf{a}_R^H(f_s)\mathbf{R}_y^{-1}\mathbf{a}_R(f_s)\right)^2}\\ &= \frac{1}{\mathbf{a}_R^H(f_s)\mathbf{R}_y^{-1}\mathbf{a}_R(f_s)}.\end{aligned} \tag{A.5}$$

Since $\mathbf{R}_y$ is invertible and $\mathbf{a}_R(f_{st})\mathbf{a}_R(f_{st})^H$ is a rank 1 matrix, the Sherman-Morrison formula is used to derive the inverse of $\mathbf{R}_y$ as follows

$$\begin{aligned}\mathbf{R}_y^{-1} &= \left(|\beta_t|^2\,\mathbf{a}_T^T(f_{st})\mathbf{R}_{xx}\mathbf{a}_T^*(f_{st})\mathbf{a}_R(f_{st})\mathbf{a}_R(f_{st})^H + \sigma_n^2\mathbf{I}_{n_R}\right)^{-1}\\ &= \frac{1}{\sigma_n^2}\mathbf{I}_{n_R} - \frac{|\beta_t|^2\,\mathbf{a}_T^T(f_{st})\mathbf{R}_{xx}\mathbf{a}_T^*(f_{st})\ \mathbf{a}_R(f_{st})\mathbf{a}_R(f_{st})^H}{\sigma_n^4 + |\beta_t|^2\,n_R\sigma_n^2\mathbf{a}_T^T(f_{st})\mathbf{R}_{xx}\mathbf{a}_T^*(f_{st})}.\end{aligned} \tag{A.6}$$

So, we can confirm that

$$\begin{aligned}&\mathbf{a}_R^H(f_s)\mathbf{R}_y^{-1}\mathbf{a}_R(f_s)\\ &= \frac{n_R}{\sigma_n^2} - \frac{|\beta_t|^2\,\mathbf{a}_T^T(f_{st})\mathbf{R}_{xx}\mathbf{a}_T^*(f_{st})\ \left|\mathbf{a}_R^H(f_s)\mathbf{a}_R(f_{st})\right|^2}{\sigma_n^4 + |\beta_t|^2\,n_R\sigma_n^2\mathbf{a}_T^T(f_{st})\mathbf{R}_{xx}\mathbf{a}_T^*(f_{st})},\end{aligned} \tag{A.7}$$

is minimized at $f_s = f_{st}$, and its inverse $\mathbf{w}^H(f_s)\mathbf{R}_y\mathbf{w}(f_s)$ is maximized at $f_s = f_{st}$ □.

In the final part of the proof, we will demonstrate by contradiction that if

$$f_{st} = \underset{f_s}{\operatorname{argmax}}\ \mathbf{w}^H(f_s)\mathbf{R}_y\mathbf{w}(f_s), \tag{A.8}$$

and

$$f_{dt}, f_{st} = \underset{f_d, f_s}{\operatorname{argmin}} \left[\mathbf{w}^H(f_s)\mathbf{R}_y\mathbf{w}(f_s) - \frac{\left|\mathrm{E}\left\{e^{-j2\pi f_d n}\mathbf{w}^H(f_s)\mathbf{y}(n)\mathbf{x}^H(n)\mathbf{a}_T^*(f_s)\right\}\right|^2}{\mathbf{a}_T^T(f_s)\mathbf{R}_{xx}\mathbf{a}_T^*(f_s)}\right], \tag{A.9}$$

then

$$\begin{aligned} f_{dt}, f_{st} &= \underset{f_d, f_s}{\operatorname{argmax}}\ \frac{\left|\mathrm{E}\left\{e^{-j2\pi f_d n}\mathbf{w}^H(f_s)\mathbf{y}(n)\mathbf{x}^H(n)\mathbf{a}_T^*(f_s)\right\}\right|^2}{\mathbf{a}_T^T(f_s)\mathbf{R}_{xx}\mathbf{a}_T^*(f_s)} \\ &= \underset{f_d, f_s}{\operatorname{argmax}}\ \left|\beta\left(f_d, f_s\right)\right|^2 \mathbf{a}_T^T(f_s)\mathbf{R}_{xx}\mathbf{a}_T^*(f_s). \end{aligned} \tag{A.10}$$

To that end, let us assume that it exits a couple of values (f_{d_e}, f_{s_e}) such that

$$\begin{aligned} &\mathbf{a}_T^T(f_{s_e})\mathbf{R}_{xx}\mathbf{a}_T^*(f_{s_e})\left|\beta\left(f_{d_e}, f_{s_e}\right)\right| \\ &\qquad > \mathbf{a}_T^T(f_{s_t})\mathbf{R}_{xx}\mathbf{a}_T^*(f_{s_t})\left|\beta\left(f_{d_t}, f_{s_t}\right)\right|. \end{aligned} \tag{A.11}$$

Using (A.8), we can write

$$\mathbf{w}^H(f_{s_e})\mathbf{R}_y\mathbf{w}(f_{s_e}) \leq \mathbf{w}^H(f_{s_t})\mathbf{R}_y\mathbf{w}(f_{s_t}), \tag{A.12}$$

which leads to

$$\begin{aligned} &\mathbf{w}^H(f_{s_e})\mathbf{R}_y\mathbf{w}(f_{s_e}) - \mathbf{a}_T^T(f_{s_e})\mathbf{R}_{xx}\mathbf{a}_T^*(f_{s_e})\left|\beta\left(f_{d_e}, f_{s_e}\right)\right|^2 \\ &< \mathbf{w}^H(f_{s_t})\mathbf{R}_y\mathbf{w}(f_{s_t}) - \mathbf{a}_T^T(f_{s_t})\mathbf{R}_{xx}\mathbf{a}_T^*(f_{s_t})\left|\beta\left(f_{d_t}, f_{s_t}\right)\right|^2. \end{aligned} \tag{A.13}$$

Because (A.13) contradicts (A.9), we can finally conclude that solving (10) is equivalent to solving (11) under the noise only assumption.

REFERENCES

[1] E. Fishler, A. Haimovich, R. Blum, R. Cimini, D. Chizhik, and R. Valenzuela, "Performance of MIMO radar systems: advantages of angular diversity," in *Conference Record of the Thirty-Eighth Asilomar Conference on Signals, Systems and Computers*, vol. 1, pp. 305–309, Nov. 2004.

[2] J. Li and P. Stoica, "MIMO radar with colocated antennas," *IEEE Signal Processing Magazine*, vol. 24, pp. 106–114, Sept. 2007.

[3] A. M. Haimovich, R. S. Blum, and L. J. Cimini, "MIMO radar with widely separated antennas," *IEEE Signal Processing Magazine*, vol. 25, pp. 116–129, Jan. 2008.

[4] E. Fishler, A. Haimovich, R. Blum, D. Chizhik, L. Cimini, and R. Valenzuela, "MIMO radar: an idea whose time has come," in *Proceedings of the IEEE Radar Conference*, pp. 71–78, Apr. 2004.

[5] E. Fishler, A. Haimovich, R. Blum, L. Cimini, D. Chizhik, and R. Valenzuela, "Spatial diversity in radars-models and detection performance," *IEEE Transactions on Signal Processing*, vol. 54, pp. 823–838, Mar. 2006.

[6] J. Li, P. Stoica, L. Xu, and W. Roberts, "On parameter identifiability of MIMO radar," *IEEE Signal Processing Letters*, vol. 14, pp. 968–971, Dec. 2007.

[7] J. Li and P. Stoica, *MIMO Radar Signal Processing - Diversity Means Superiority*. Hoboken New Jersey: John Wiley & Sons, Inc., 2008.

[8] L. Xu, J. Li, and P. Stoica, "Target detection and parameter estimation for MIMO radar systems," *IEEE Transactions on Aerospace and Electronic Systems*, vol. 44, pp. 927–939, July 2008.

[9] A. Hassanien, S. Vorobyov, and A. Gershman, "Moving Target Parameters Estimation in Noncoherent MIMO Radar Systems," *IEEE Transactions on Signal Processing*, vol. 60, pp. 2354–2361, May 2012.

[10] F. Liu and J. Wang, "AD-MUSIC for jointly DOA and DOD estimation in bistatic MIMO radar system," in *2010 International Conference on Computer Design and Applications*, vol. 4, pp. V4–455–V4–458, June 2010.

[11] M. Jin, G. Liao, and J. Li, "Joint DOD and DOA estimation for bistatic MIMO radar," *Signal Processing*, vol. 89, no. 2, pp. 244 – 251, 2009.

[12] M. Bencheikh and Y. Wang, "Joint DOD-DOA estimation using combined ESPRIT-MUSIC approach in MIMO radar," *Electronics Letters*, vol. 46, pp. 1081–1083, July 2010.

[13] K. Rambach and B. Yang, "Direction of Arrival estimation of two moving targets using a time division multiplexed colocated MIMO radar," in *IEEE Radar Conference*, pp. 1118–1123, May 2014.

[14] K. Rambach and B. Yang, "Colocated MIMO radar: Cramer-Rao bound and optimal time division multiplexing for DOA estimation of moving targets," in *IEEE International Conference on Acoustics, Speech and Signal Processing (ICASSP)*, pp. 4006–4010, May 2013.

[15] M. Xue, W. Roberts, J. Li, X. Tan, and P. Stoica, "MIMO radar sparse angle-Doppler imaging for ground moving target indication," in *2010 IEEE Radar Conference*, pp. 553–558, May 2010.

[16] J. Capon, "High-resolution frequency-wavenumber spectrum analysis," *Proceedings of the IEEE*, vol. 57, no. 8, pp. 1408–1418, 1969.

[17] H. Krim and M. Viberg, "Two decades of array signal processing research: the parametric approach," *IEEE Signal Processing Magazine*, vol. 13, pp. 67–94, July 1996.

[18] P. Stoica, H. Li, and J. Li, "A new derivation of the APES filter," *IEEE Signal Processing Letters*, vol. 6, pp. 205–206, Aug. 1999.

[19] C. Richmond, "On the probability of resolution for the amplitude and phase estimation (APES) spectral estimator," in *IEEE International Conference on Acoustics, Speech, and Signal Processing*, vol. 4, pp. 1025–1028, Mar. 2005.

[20] G. H. Golub and C. F. Van Loan, *Matrix Computations (3rd Ed.)*. Baltimore, MD, USA: Johns Hopkins University Press, 1996.

[21] P. Stoica and R. Moses, *Introduction to Spectral Analysis*. Prentice Hall, 1997.

[22] S. Jardak, S. Ahmed, and M.-S. Alouini, "Low complexity joint estimation of reflection coefficient, spatial location, and Doppler shift for MIMO radar by exploiting 2D-FFT," *International Radar Conference, Lille, France*, Oct. 2014.

[23] S. Jardak, S. Ahmed, and M. Alouini, "Generation of correlated finite alphabet waveforms using gaussian random variables," *IEEE Transactions on Signal Processing*, vol. 62, no. 17, pp. 4587–4596, 2014.

[24] D. Bliss and K. Forsythe, "Multiple-input multiple-output (MIMO) radar and imaging: degrees of freedom and resolution," in *Conference Record of the Thirty-Seventh Asilomar Conference on Signals, Systems and Computers, 2004.*, vol. 1, pp. 54–59, Nov. 2003.

[25] K. Forsythe, D. Bliss, and G. S. Fawcett, "Multiple-input multiple-output (MIMO) radar: performance issues," in *Conference Record of the Thirty-Eighth Asilomar Conference on Signals, Systems and Computers*, vol. 1, pp. 310–315, Nov. 2004.

[26] D. J. Rabideau and P. Parker, "Ubiquitous MIMO multifunction digital array radar," in *Conference Record of the Thirty-Seventh Asilomar Conference on Signals, Systems and Computers, 2004.*, vol. 1, pp. 1057–1064, Nov. 2003.

[27] F. Robey, S. Coutts, D. Weikle, J. McHarg, and K. Cuomo, "MIMO radar theory and experimental results," in *Conference Record of the Thirty-Eighth Asilomar Conference on Signals, Systems and Computers*, vol. 1, pp. 300–304, Nov. 2004.

[28] L. Xu, J. Li, and P. Stoica, "Radar Imaging Via Adaptive MIMO Techniques," in *14th European Signal Processing Conference (EUSIPCO 2006), Florence, Italy, Sept. 2006*.